Magnetic properties of AlN monolayer doped with group 1A or 2A nonmagnetic element: First-principles study*

Ruilin Han(韩瑞林)[1,†], Xiaoyang Chen(陈晓阳)[1], and Yu Yan(闫羽)[2]

[1] College of Physics and Electronic Engineering, Shanxi University, Taiyuan 030006, China
[2] Key Laboratory of Physics and Technology for Advanced Batteries (Ministry of Education), Department of Physics, Jilin University, Changchun 130012, China

(Received 26 April 2017; revised manuscript received 16 June 2017; published online 18 July 2017)

The electronic structure, magnetic properties, and mechanism of magnetization in two-dimensional (2D) aluminum nitride (AlN) monolayer doped with nonmagnetic elements of group 1A (Li, Na, K) or group 2A (Be, Mg, Ca) were systematically investigated using first-principles studies. Numerical results reveal that the total magnetic moments produced by group 1A and group 2A nonmagnetic doping are $2.0\mu_B$ and $1.0\mu_B$ per supercell, respectively. The local magnetic moments of the three N atoms around the doping atom are the primary moment contributors for all these doped AlN monolayers. The p orbital of the dopant atom contributes little to the total magnetic moment, but it influences adjacent atoms significantly, changing their density of states distribution, which results in hybridization among the p orbitals of the three closest N atoms, giving rise to magnetism. Moreover, the doped AlN monolayer, having half-metal characteristics, is a likely candidate for spintronic applications. When two group 1A or group 2A atoms are inserted, their moments are long-range ferromagnetically coupled. Remarkably, the energy of formation shows that, if the monolayer has been grown under N-rich conditions, substitution of a group 2A atom at an Al site is easier than substitution of a group 1A atom.

Keywords: AlN nanosheets, ferromagnetism, first-principles, doping

PACS: 75.50.Gg, 75.50.Pp, 75.75.Lf **DOI:** 10.1088/1674-1056/26/9/097503

1. Introduction

Exploration of two-dimensional (2D) materials is a hot topic these days — including new dilute magnetic semiconductor materials — because such materials have extraordinary physicochemical properties and may well be useful in electronic and spintronic devices.[1–12] The advantages of aluminum nitride (AlN), an important wide-band-gap semiconductor, are attracting wide interest — the same honeycomb lattice structure as graphene, high thermal conductivity, little thermal expansion, and good chemical stability. Hence, it is already used in photoelectronics,[13] optics,[14] electronics,[15,16] and spintronics.[17–23] In particular, the AlN-based dilute magnetic semiconductor material is considered as the most promising candidate for future spintronic and spin-magnetic devices.

Since pristine monolayer AlN has no intrinsic magnetism as a semiconductor, considerable effort has been devoted to inducing magnetism. Intrinsic vacancy defects, doping, adsorption, applied stress, and an additional substrate have each been proved to be efficient and promising alterations to produce magnetism in the material. Among these alterations, substitutional doping has been proposed to be the most efficient, and it is widely used to produce and tune the magnetic states. For example, theoretical calculations indicated that ferromagnetism in an AlN nanosheet can be obtained by doping with transition metal (TM) impurities.[24] Nevertheless, researchers also reported strong evidence of magnetic clusters or secondary phases, suggesting that the overall behavior of the modified material is an obstacle for practical applications.[25,26] So much effort has been invested in exploring the effects of nonmagnetic element dopants. Fan *et al.*[27] revealed that substituting B for N can produce magnetization, and a double-exchange mechanism is important in forming the ferromagnetism. Bai *et al.*[28] demonstrated that Be and C dopants can produce local spin states, resulting in a magnetic moment of $1.00\mu_B$. Experimental and theoretical studies showed that Cu doped AlN nanorods, films, and powders exhibit room temperature ferromagnetism.[29–32] In addition, it was predicted experimentally that Zn can be incorporated into an AlN solid solution,[33] and correspondingly, it has been confirmed theoretically that Zn/Cd doping can induce magnetism in an AlN nanosheet.[34] To date, in contrast with the wide study of the electronic structure and magnetic properties of doped monolayer AlN, the effects of group 1A and group 2A dopants in monolayer AlN have not been investigated. Therefore, this paper focuses on the electronic structures, magnetic properties, and the mechanism of magnetization in an AlN monolayer doped with group 1A and 2A nonmagnetic elements X (X = Li, Na, K, Be, Mg, Ca), within the framework of first-principles studies.

*Project supported by the National Fundamental Fund of Personnel Training, China (Grant No. J1103210).
†Corresponding author. E-mail: hanruilin0116@sxu.edu.cn
© 2017 Chinese Physical Society and IOP Publishing Ltd

2. Computational method and details

The calculations of electronic structure and ionic relaxation were prepared within the framework of density functional theory, based on the projector augmented wave method, as implemented in the Vienna *ab-initio* simulation package (VASP).[35,36] The cutoff energy for the plane wave basis was 400 eV, the exchange and correlation effects were treated with the Perdew–Wang generalized gradient approximation (GGA), and the ion–electron interaction was depicted through the projector augmented plane wave potentials.[37,38] A vacuum layer space of 15 Å was set to preclude interaction between adjacent monolayers. All the structures were fully relaxed to minimize the total energy of the systems until it converged at the threshold of 10^{-5} eV and the force on each atom was less than 0.02 eV/Å. In addition, the Heyd–Scuseria–Ernzerhof (HSE06) functional[39] was adopted to check the electronic structure. As shown in Figs. 1(b) and (c), the model was a 32-atom (4×4×1) supercell of $Al_{16}N_{16}$, having the wurtzite structure to simulate the electronic structure and magnetic properties. A larger 6×6×1 supercell, including 72 atoms, was chosen to simulate ferromagnetic coupling calculations; 9×9×1 and 5×5×1 Monkhorst-Pack meshes were used respectively to sample the Brillouin zone for the structural relaxations and physical properties of the single-atom-doped case and two-dopant case.

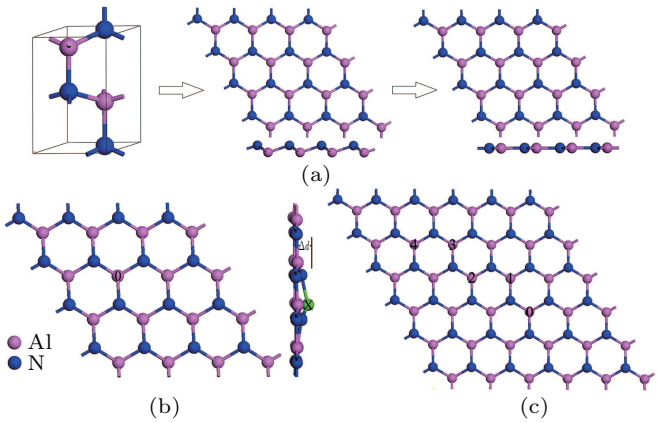


Fig. 1. (color online) (a) A unit cell cut directly into the (0001) plane of optimized bulk wurtzite AlN ($a = 3.126$ Å and $c = 5.017$ Å) structure. (b) Schematic view of structure for 4×4×1 AlN nanosheet surpercells, and the distance (Δd) between X atom and AlN nanosheet plane. (c) Schematic view of structure for 6×6×1 AlN nanosheet supercells. Pink and dark blue spheres represent Al and N atoms, respectively. We use i to indicate the dopant pair, X (0, i), depicted in Fig. 1(c), in which the first dopant atom occupies the fixed Al position, labeled 0 in Fig. 1(c), and the second dopant atom occupies the positions indicated by $i = 1$–4.

3. Results and discussion

In order to obtain exactly a 2D AlN monolayer, we cut a unit cell directly into the (0001) plane of an optimized bulk wurtzite AlN ($a = 3.126$ Å and $c = 5.017$ Å) structure. With relaxation of the electronic structure, the 2D AlN monolayer changes from a rippled surface to a planar graphene-like structure, as shown in Fig. 1(a). In addition, the relaxed Al–N bond length, 1.785 Å, in the case of a monolayer is shorter than the 1.898 Å bond length in the bulk structure, consistent with previous results.[17,40] The sp^2 bonding between Al and N atoms in the monolayer is found to be stronger than the tetrahedral coordinated sp^3 bonding in the bulk. The spin-polarized density of states (DOS) of the pristine AlN monolayer indicates that no spin polarization occurs in either the majority-spin channel or the minority-spin channel, as shown in Fig. 2(a), suggesting a pure AlN monolayer is intrinsically nonmagnetic. As shown in Fig. 2(b), the band structure of a pure AlN monolayer exhibits an indirect band gap of 2.95 eV. Considering that a GGA functional describes orbit localization poorly, and the most typical problem is underestimating the band gap, we also adopted the HSE06 functional to check the energy gap of the pristine 2D AlN monolayer. As shown in Fig. 2(c), the revised energy gap value is 4.06 eV. All above results are in good agreement with previous theoretical results,[21,41–43] suggesting the reliability of our computational methods.

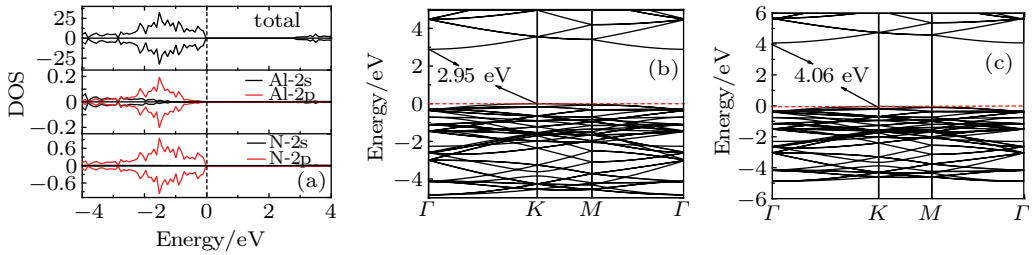


Fig. 2. (color online) (a) Total DOS and partial DOS of p and s states for the Al atoms and N atoms, (b) band structure for pure 2D AlN nanosheets calculated by GGA, and (c) band structure for pure 2D AlN nanosheets calculated by HSE06. The Fermi energy is indicated by the dotted line.

Next, we begin to investigate the doped monolayer AlN systems $Al_{15}XN_{16}$ (X = Li, Na, K, Be, Mg, Ca), in which one Al atom in the monolayer is replaced by one dopant X atom, labeled as 0 (impurity concentration of 6.25%), as shown in Fig. 1(b). In order to evaluate the stability of the doped $Al_{15}XN_{16}$ system, the formation energy E_{form} of the $Al_{15}XN_{16}$ monolayer is analyzed. The formation energy is defined as the energy difference between the doped $Al_{15}XN_{16}$

system, pristine AlN monolayer, and the total energy of metallic Al and X atoms, respectively. The formation energy is expressed as $E_{\rm form} = E(Al_{15}XN_{16})$–$E(Al_{16}N_{16}) + \mu_{Al} - \mu_X$.[44] It should be noted that the formation energy depends on the Al-rich vs. N-rich condition. Under the thermodynamic growth conditions, the upper and lower limits for the chemical potentials μ_N and μ_{Al} of N and Al are obtained from the equation $\mu_{Al} + \mu_N = \Delta H_f(AlN)$, where $\Delta H_f(AlN)$ is the formation enthalpy of AlN nanosheets. The calculated data under both Al-rich and N-rich conditions are listed in Table 1, which shows that a dopant atom is more likely to occupy an Al site in the N-rich condition than in the Al-rich condition. Our calculated results indicate that X (X = Li, Na, K, Be, Mg, Ca) atoms can easily be implanted in the Al site of monolayer AlN if the sample is grown under N-rich conditions. Moreover, the Al atom is more likely to be replaced by group 2A nonmagnetic elements than group 1A atoms. Table 1 also summarizes the total energy difference between the spin polarized and non-spin polarized states for $Al_{15}XN_{16}$ (X = Li, Na, K, Be, Mg, Ca), i.e., $\Delta E_{\rm Spin} = E_{\rm sp} - E_{\rm nsp}$. As listed in Table 1, all of the calculated total energies of $\Delta E_{\rm Spin}$ are negative for group 1A or 2A nonmagnetic element doped AlN monolayer, which suggests that the spin polarized state is energetically more favorable, and the ground state of the $Al_{15}XN_{16}$ (X = Li, Na, K, Be, Mg, Ca) monolayer is magnetic.

Table 1. Calculated energy difference between the spin polarized and non-spin polarized states, and the formation energies $E_{\rm form}$ of X (X = Li, Na, K, Be, Mg, Ca) doped AlN monolayers in Al-rich and N-rich conditions.

System	$\Delta E_{\rm Spin}$/eV	$E_{\rm form}$/eV	
		Al-rich	N-rich
$Al_{15}LiN_{16}$	–0.014	5.673	4.332
$Al_{15}NaN_{16}$	–0.015	6.411	4.401
$Al_{15}KN_{16}$	–0.015	6.407	4.397
$Al_{15}BeN_{16}$	–0.002	2.217	0.877
$Al_{15}MgN_{16}$	–0.002	3.350	2.010
$Al_{15}CaN_{16}$	–0.003	1.892	0.552

The optimized bond lengths of X–N (X = Li, Na, K, Be, Mg, Ca), the local magnetic moment of dopant X with its nearby N atoms, and the total magnetic moment of the monolayer are summarized in Table 2, which shows that the optimized bond lengths of X–N (X = Li, Na, K, Be, Mg, Ca) are 1.988 Å, 2.305 Å, 2.667 Å, 1.689 Å, 1.937 Å, and 2.255 Å, respectively, which are all larger (except Be) than the pristine Al–N bond length of 1.785 Å. Also from Table 2, we see that the distance (Δd) between the AlN nanosheet and the dopant atom X is larger when the bond length is larger: the Δd values of the $Al_{15}XN_{16}$ (X = Li, Na, K, Be, Mg, Ca) monolayer are 1.055 Å, 1.806 Å, 2.392 Å, 1.174 Å, 1.816 Å, and 1.235 Å, respectively. These phenomena are attributed mainly to the fact that the ionic radii of Li (0.68), Na (0.97), K (1.33), Mg (0.66), and Ca (0.99) are larger than that of Al (0.51); however, the ionic radius of Be (0.35) is shorter than that of Al. In addition, note that the X–N bond lengths follow the order Li–N<Na–N<K–N and Be–N<Mg–N<Ca–N. It can also be explained by the difference of the ionic radii of the Al cation and the X cation (X = Li, Na, K, Be, Mg, Ca). Besides the optimized bond lengths of X–N (X = Li, Na, K, Be, Mg, Ca), we also consider the bond lengths of other Al atoms and N atoms around the dopant atom. The bond length changes in the Li doped AlN monolayer are taken as an example, as shown in Fig. 3(a), where it can be seen that the elongation of the X–N bonds distorts the pristine AlN monolayer lattice slightly, and the corresponding bond lengths of other Al atoms and N atoms around the dopant atom also change slightly, resulting in other slight structural distortions. For other atoms (Na, K, Be, Mg, Ca), the variation of the Al–N bond length is similar to that for Li doping. The local magnetic moments of each doping atom, the three N atoms nearest to the dopant, and the total magnetic moments of the $Al_{15}XN_{16}$ (X = Li, Na, K, Be, Mg, Ca) monolayer are listed in Table 2, where we see that the total magnetic moment of the $Al_{15}XN_{16}$ monolayer is either $2.000\mu_B$, induced by Li, Na, or K, or $1.000\mu_B$, induced by Be, Mg, or Ca. This result is not difficult to understand, because the group 1A or 2A nonmagnetic elements X have one or two valence electrons while the host Al has three. This makes the calculated total magnetic moment exactly equal to the number of produced holes in the $Al_{15}XN_{16}$ (X = Li, Na, K, Be, Mg, Ca) monolayer. The dopant X atom (X = Li, Na, K, Be, Mg, Ca) in the monolayer provides a small part of the magnetic moment. It can even be said that the contribution of the dopant atoms to the total magnetic moment is almost zero for the $Al_{15}XN_{16}$ monolayer. The magnetic moments of the nearest neighbor N atoms around the dopant atom account for most of the total magnetic moment. The residual magnetic moment is distributed in the interstitial region between the dopant atom and its nearest atoms. The DOS and partial DOS in Fig. 4 and the spin density distributions in Fig. 5 confirm the above view.

Table 2. Optimized X–N bond length (X = Li, Na, K, Be, Mg, Ca). The distance (Δd) between the AlN nanosheet and the dopant atom X. Magnetic moment of the doping atom (M_X), its nearest neighboring N atoms (M_N) around the doping atom, and the total magnetic moment of the nanosheets ($M_{\rm tot}$).

System	X–N/Å	Δd/Å	M_X/μ_B	M_N/μ_B	$M_{\rm tot}/\mu_B$
$Al_{15}LiN_{16}$	1.988	1.055	0.009	1.077	2.000
$Al_{15}NaN_{16}$	2.305	1.806	0.003	1.119	2.000
$Al_{15}KN_{16}$	2.667	2.392	0.002	1.130	2.000
$Al_{15}BeN_{16}$	1.689	1.174	0.011	0.430	1.000
$Al_{15}MgN_{16}$	1.937	1.816	0.003	0.388	1.000
$Al_{15}CaN_{16}$	2.255	1.235	0.035	0.474	1.000

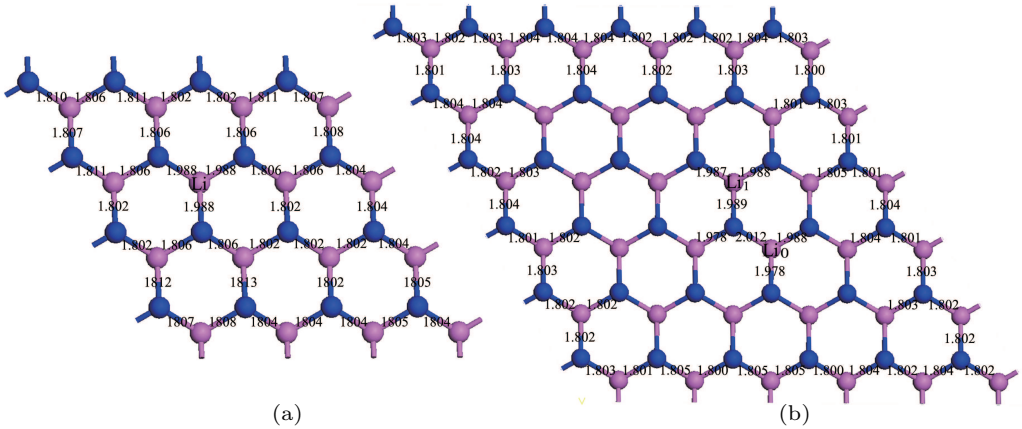


Fig. 3. (color online) (a) Bond length changes of $Al_{15}LiN_{16}$ monolayer and (b) variation of the Al–N bond length near the boundary of $Al_{34}Li_2N_{36}$ monolayer. The unit of bond length is Å.

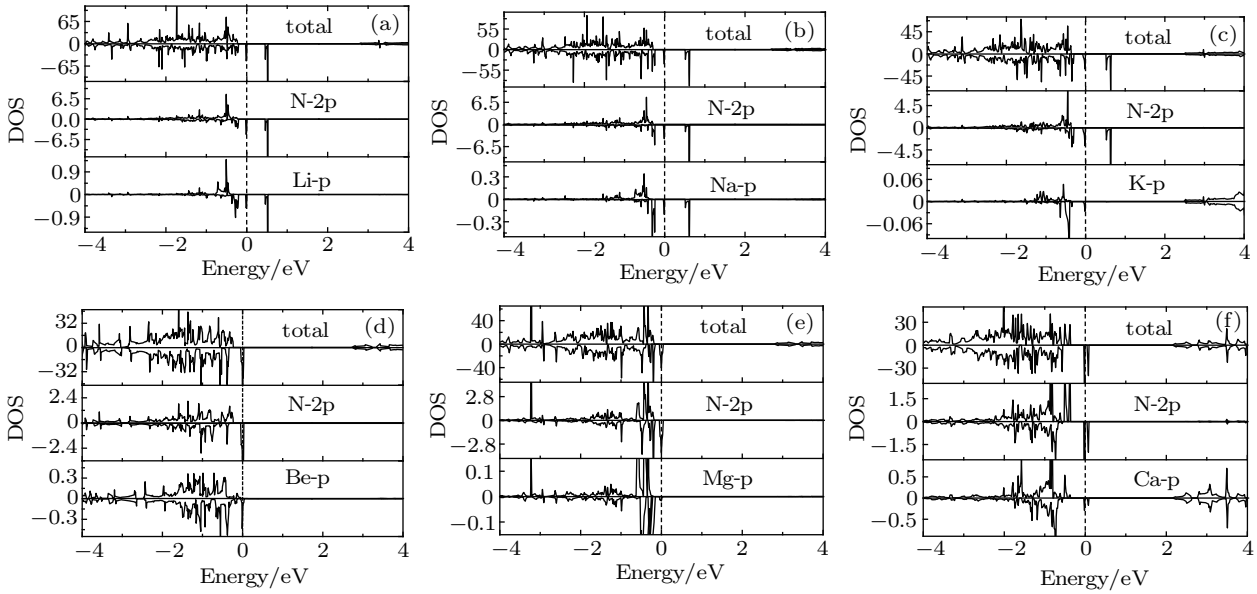


Fig. 4. Total density of states (TDOS) of $Al_{15}XN_{16}$ (X = Li, Na, K, Be, Mg, Ca) monolayer, partial density of states (PDOS) of dopant X (X = Li, Na, K, Be, Mg, Ca), and p states of a nearest-neighbor N atom around dopant X.

Figure 4 presents the total density of states (TDOS) of each $Al_{15}XN_{16}$ (X = Li, Na, K, Be, Mg, Ca) monolayer, the partial density of states (PDOS) of the dopant X (X = Li, Na, K, Be, Mg, Ca), and p states of one of the first neighboring N atoms around dopant X. From Fig. 4, it is easy to see that the distribution of the electronic states for majority-spin and minority-spin orbits is asymmetric. The splitting of states near the Fermi energy consists mainly of the 2p states of the first neighboring N atoms around the dopant X. The dopant X atom contributes very little to the moment. Together, this information implies that monolayer AlN doped with group 1A or 2A atoms exhibits magnetic ground states. The result in the $Al_{15}XN_{16}$ monolayer is 2.000μ_B if induced by Li, Na, or K, or 1.000μ_B if induced by Be, Mg, or Ca. The origin of the magnetic moment can be explained as follows: low-valence-state X (X = Li, Na, K, Be, Mg, Ca) substituted for an Al atom brings about a slight deformation of the crystal structure, which makes the symmetric hexagonal structure of 2D AlN monolayer transform to bulk AlN structure with T_d symmetry. Since we know that each N atom around the Al atom has three valence electrons, and the N^{3-} anion has six p electrons with no unpaired electrons, the first three nearest-neighbor N atoms of the Al atom nominally carry 18 p-electrons in total. By Bader analysis, we find that the three nearest-neighbor N atoms of the dopant atom carry 16 p-electrons and 17 p-electrons in total for monolayer AlN doped with group 1A or 2A atoms. This means that substitutional doping of monolayer AlN by low-valence-state X (X = Li, Na, K, Be, Mg, Ca) brings about some holes in the 2p orbitals of the N atoms, making the total magnetic moment of the $Al_{15}XN_{16}$ monolayer either 2.000μ_B induced by Li, Na, or K, or 1.000μ_B induced by Be, Mg, or Ca. Furthermore, the calculated magnetic moment is equal to the number of holes produced by the dopant atom. From Fig. 4, one can also see that the minority-spin orbits at

the top of the valence band for monolayer $Al_{15}XN_{16}$ (X = Li, Na, K, Be, Mg, Ca) clearly pass through the Fermi level, indicating that the doped monolayers are half-metallic materials, which might well be advantageous candidates for spintronic devices in magnetic fields. Figure 5 shows the spatial distribution of spin density for relaxed $Al_{15}XN_{16}$ (X = Li, Na, K, Be, Mg, Ca). The plot in Fig. 5, reveals that in most of these cases, the spin densities are localized in the first three neighboring N atoms around the X dopant atom. The more remote N atoms provide only a little, but they influence the adjacent atoms significantly and influence the density of states distribution. The contribution of the dopant atoms to the total magnetic moment is almost zero for the $Al_{15}XN_{16}$ monolayer, in agreement with the magnetic moment distribution. These characteristics manifest a very strong hybridization among the three N atoms near the dopant atom in the monolayer, which implies that the p–p exchange among these N atoms could be the origin of the magnetism.

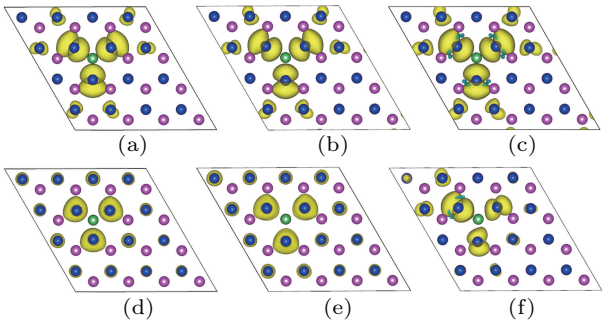


Fig. 5. (color online) Spatial distribution of spin density in relaxed (a) $Al_{15}LiN_{16}$, (b) $Al_{15}NaN_{16}$, (c) $Al_{15}KN_{16}$, (d) $Al_{15}BeN_{16}$, (e) $Al_{15}MgN_{16}$, (f) $Al_{15}CaN_{16}$. Yellow and blue isosurfaces correspond to the majority- and minority-spin densities. Pink and dark blue balls represent Al and N atoms, respectively. Position of the dopant atom is marked as green. The isosurface value of spin charge is 0.0007 e·Å^{-3}.

Now we focus the discussion on the magnetic coupling between the moments induced by two dopant X (X = Li, Na, K, Be, Mg, Ca) atoms (doping concentration is 5.6%). We replace two Al atoms by X atoms in the larger 6×6×1 AlN monolayer. To judge whether the selected cell size is reasonable or not, we give the variation of the Al–N bond length near the boundary of $Al_{34}Li_2N_{36}$ monolayer, as shown in Fig. 3(b). The results show that the larger ionic radius of X dopants (with respect to Al) results in elongation of the X–N bonds and distortion of local structures. The length of the Al–N bond near the boundary of the $Al_{34}Li_2N_{36}$ monolayer is almost the same as the length of the Al–N bond (1.802 Å) in the pristine AlN. Moreover, for the $Al_{34}X_2N_{36}$ (X = Na, K, Be, Mg, Ca) monolayer, the variation of the Al–N bond length is similar to that with Li doping, which implies that our cell size is reasonable. Four possible and independent configurations of the two X (X = Li, Na, K, Be, Mg, Ca) atoms are considered. We use i to indicate the dopant pair X (0, i) depicted in Fig. 1(c), in which the first dopant atom is fixed, labeled 0 in Fig. 1(c), and the second dopant atom occupies the position indicated by i = 1–4. For each configuration, we consider the spin-polarized calculations, ferromagnetic (FM), and antiferromagnetic (AFM) coupling between the moments induced by the two dopant atoms. The calculated results of the distance between the two dopant X atoms (d_{X-X}), relative energy ($\Delta\varepsilon$) with respect to the (0, 1) configuration, difference between the FM energy and the AFM energy ($\Delta E_m = E_{FM} - E_{AFM}$), and total magnetic moment for all the configurations of the doped system are also listed in Table 3. The calculations show that ΔE_m of each configuration is negative, suggesting all ground states of $Al_{34}X_2N_{36}$ (X = Li, Na, K, Be, Mg, Ca) are FM. More importantly, it can be seen from Table 3 that the ΔE_m values of all the (0, 4) configurations with a large distance (d_{X-X} = 10.829 Å) between the two dopant X atoms are negative. The ΔE_m of the (0, 4) configuration for AlN monolayer doped with Li, Na, or K is a small negative value, which still implies that ferromagnetism is likely achieved in the AlN monolayer by doping group 1A or 2A atoms. Furthermore, the magnetic moment induced by each dopant X element in the FM or AFM state is almost the same as that of the $Al_{15}XN_{16}$ monolayer. In addition, based on the mean-field theory, the Curie temperatures of the (0, 4) configuration for the X-doped AlN monolayer (X = Li, Na, K, Be, Mg, Ca) are estimated and analyzed by formula $\gamma\kappa_B T_C/2 = (E_{AFM} - E_{FM})$, where γ and κ_B are, respectively, the dimension of the system and the Boltzmann constant.[45] For the X-doped AlN monolayer (X = Li, Na, K, Be, Mg, Ca), our estimated Curie temperatures are 45 K,

Table 3. Calculated distance (d_{X-X}) between two dopants; relative energy $\Delta\varepsilon$ with respect to the (0, 1) structure; energy difference (ΔE_m) between FM and AFM states, $\Delta E_m = E_{FM} - E_{AFM}$; and total magnetic moment (M_{tot}) in FM state for doped system $Al_{34}X_2N_{36}$ (X = Li, Na, K, Be, Mg, Ca).

System	Configuration (0, i)	d_{X-X}/Å	ΔE_m/meV	$\Delta\varepsilon$/meV	M_{tot}/μ_B
$Al_{34}Li_2N_{36}$	(0,1)	3.126	–365.8	0.00	4.00
	(0,2)	5.414	–71.5	294.3	4.00
	(0,3)	8.271	–14.2	351.6	4.00
	(0,4)	10.829	–3.9	361.9	4.00
$Al_{34}Na_2N_{36}$	(0,1)	3.126	–383	0.00	4.00
	(0,2)	5.414	–150.1	232.9	4.00
	(0,3)	8.271	–11.2	371.8	4.00
	(0,4)	10.829	–9.6	373.4	4.00
$Al_{34}K_2N_{36}$	(0,1)	3.126	–599.9	0.00	4.00
	(0,2)	5.414	–446.8	153.1	4.00
	(0,3)	8.271	–38.2	561.7	4.00
	(0,4)	10.829	–15.7	584.2	4.00
$Al_{34}Be_2N_{36}$	(0,1)	3.126	–258.6	0.00	2.00
	(0,2)	5.414	–101.7	156.9	2.00
	(0,3)	8.271	–76.6	182	2.00
	(0,4)	10.829	–59.7	198.9	2.00
$Al_{34}Mg_2N_{36}$	(0,1)	3.126	–329.5	0.00	2.00
	(0,2)	5.414	–153.3	176.2	2.00
	(0,3)	8.271	–128.1	201.4	2.00
	(0,4)	10.829	–122.1	207.4	2.00
$Al_{34}Ca_2N_{36}$	(0,1)	3.126	–233.9	0.00	2.00
	(0,2)	5.414	–139.9	94	2.00
	(0,3)	8.271	–133.2	90.7	2.00
	(0,4)	10.829	–66.4	167.5	2.00

111 K, 182 K, 693 K, 1416 K, and 770 K, respectively, when the AlN monolayer is treated as a 2D system. In addition, the calculated total energy is lowest for the (0, 4) configuration. So the X-doped AlN systems may be good ferromagnetic materials for room-temperature spintronic applications.

We can explain the origin of long-range magnetic coupling between the magnetic moments produced by two dopant atoms through the calculated DOS of a single-X-atom doped monolayer and spin density spatial distribution maps of a two-X-atom doped monolayer. The DOS and PDOS plotted in Fig. 4 reveal that the p state of the dopant X atom (X = Li, Na, K, Be, Mg, Ca) and the p states of the nearest N atoms around the dopant significantly overlap near the Fermi level. This indicates that p–p hybridization interaction occurs between the group 1A or 2A dopant and its neighboring N atoms.[46] In addition, the nearest three N atoms around the dopant X atom have similar PDOSs. This suggests that there is a stronger p–p hybridization interaction among the p states of the N atoms around the dopant X atom (X = Li, Na, K, Be, Mg, Ca). Under this strong p–p hybridization interaction, the holes produced in the p states of the N atoms around the dopants in the monolayer can couple with each other.[46,47] Indeed, the calculated spin density in Fig. 6 shows that the N atoms between two dopant atoms are polarized to different degrees, depending on their orientation and distance relative to the X site. Furthermore, the spins of the N atoms and the dopant have the same polarization direction under the p–p interaction. Meanwhile, the spatially extended p states of the N atoms extend spin alignment to several neighboring N shells around the dopant. In other words, the first neighboring N atom and the second neighboring N atom are arranged parallel to each other under extended p–p interaction, which facilitates long-range FM coupling between the two dopant atoms.

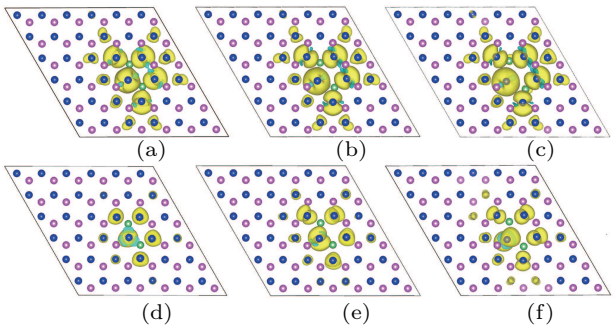


Fig. 6. (color online) Spatial distribution of spin density in relaxed (a) $Al_{34}Li_2N_{36}$, (b) $Al_{34}Na2N_{36}$, (c) $Al_{34}K_2N_{36}$, (d) $Al_{34}Be_2N_{36}$, (e) $Al_{34}Mg_2N_{36}$, (f) $Al_{34}Ca_2N_{36}$. Yellow and blue isosurfaces correspond to the majority- and minority-spin densities. Pink and dark blue balls represent Al and N atoms, respectively. Position of the dopant atom is marked as green. The isosurface value of spin charge is 0.0007 e·Å^{-3}.

4. Conclusion

We have systematically investigated the electronic, structural, and magnetic properties of group 1A and group 2A nonmagnetic-element doped AlN monolayers with 6.25% or 5.6% X (X = Li, Na, K, Be, Mg, Ca) concentration using the first-principles methodology. The calculations show that the doping energetically favors N-rich conditions as compared with Al-rich conditions. Doping with group 2A elements is easier to realize than doping with group 1A elements, indicating that a group 2A atom doped AlN monolayer can be achieved under N-rich experimental conditions. Numerical results reveal that group 1A and 2A atoms can produce magnetic properties, and the corresponding magnetic moments are $2.0\mu_B$ and $1.0\mu_B$ per supercell, respectively. The magnetic moment originates mainly from the three nearest-neighbor N atoms of the dopant X atom. Moreover, the magnetic moments are equal to the number of holes induced by the dopant atom. In addition, group 1A or 2A atom dopant AlN monolayers exhibit half-metallic ferromagnetism. More importantly, the magnetic coupling between magnetic moments introduced by double X (X = Li, Na, K, Be, Mg, Ca) atoms are FM. A p–p hybridization interaction is responsible for the long-range FM coupling. We believe that the above results are helpful for further study of the properties and applications of AlN monolayers.

References

[1] Wei R, Hu J, Zhou T, Zhou X, Liu J and Li J 2014 *Acta Mater.* **66** 163
[2] Chen P, Su Y, Liu H and Wang Y 2013 *ACS Appl. Mater. Interfaces* **5** 12073
[3] Dai J and Zeng X C 2015 *Angew. Chem. Int. Ed.* **54** 7572
[4] Iyikanat F, Sahin H, Senger R T and Peeters F M 2015 *J. Phys. Chem. C* **119** 10709
[5] Peng X Y and Ahuja R 2009 *Appl. Phys. Lett.* **94** 102504
[6] Tsipas P, Kassavetis S, Tsoutsou D, Xenogiannopoulou E, Golias E, Giamini S A, Grazianetti C, Chiappe D, Molle A, Fanciulli M and Dimoulas A 2013 *Appl. Phys. Lett.* **103** 251605
[7] Chen Z P, He J J, Zhou P, Na J and Sun L Z 2015 *Comput. Mater. Sci.* **110** 102
[8] Andriotis A N and Menon M 2014 *Phys. Rev. B* **90** 125304
[9] Zhao X, Dai X Q, Xia C X, Wang T X and Peng Y T 2015 *Solid State Commun.* **215–216** 1
[10] Ma Y D, Dai Y, Guo M, Niu C W, Lu J B and Huang B B 2011 *Phys. Chem. Chem. Phys.* **13** 15546
[11] Zhao X, Xia C X, Wang T X, Peng Y T and Dai X Q 2015 *J. Alloys Compd.* **649** 357
[12] Zhang H, Fan X L, Yang Y and Xiao P 2015 *J. Alloys Compd.* **635** 307
[13] Liu P, Sarkar A D and Ahuja R 2014 *Comput. Mater. Sci.* **86** 206
[14] Valedbagi S, Fathalian A and Elahi S M 2013 *Opt. Commun.* **309** 153
[15] He H, Huang L, Xiao M, Fu Y, Shen X and Zeng J 2013 *J. Mater. Sci.: Mater. Electron.* **24** 4499
[16] Peng Y T, Xia C X, Zhang H, Wang T X, Wei S Y and Jia Y 2014 *J. Appl. Phys.* **116** 044306
[17] Shi C M, Qin H W, Zhang Y J, Hu J F and Ju L 2014 *J. Appl. Phys.* **115** 053907
[18] Fan S W, Li W B, Huang X N, Li Z B and Pan L Q 2015 *Appl. Phys. Express* **8** 045802
[19] Bai Y J, Deng K M and Kan E J 2015 *RSC Adv.* **5** 18352
[20] Xiong J, Guo P, Guo F, Sun X and Gu H 2014 *Mater. Lett.* **117** 276
[21] Zhang C W 2012 *J. Appl. Phys.* **111** 043702
[22] Zhang W X, Li T, Gong S B, He C and Duan L 2015 *Phys. Chem. Chem. Phys.* **17** 10919
[23] He H, Huang L, Xiao M, Fu Y, Shen X and Zeng J 2013 *J. Mater. Sci.: Mater. Electron.* **24** 4499
[24] Shi C M, Qin H W, Zhang Y J, Hu J F and Ju L 2014 *J. Appl. Phys.* **115** 053907

[25] Ney A, Ollefs K, Ye S, Kammermeier T, Ney V, Kaspar T C, Chambers S A, Wilhelm F and Rogalev A 2008 *Phys. Rev. Lett.* **100** 157201
[26] Kaspar T C, Droubay T, Heald S N, Nachimuthu P, Wang C M, Shutthanandan V, Johnson C A, Gamelin D R and Chambers S A 2008 *New J. Phys.* **10** 055010
[27] Fan S W, Li W B, Huang X N, Li Z B and Pan L Q 2015 *Appl. Phys. Express* **8** 045802
[28] Bai Y J, Deng K M and Kan E J 2015 *RSC Adv.* **5** 18352
[29] Ji X H, Lau S P, Yu S F, Yang H Y, Herng T S and Chen J S 2007 *Nanotechnology* **18** 105601
[30] Li H, Chen X L, Song B, Bao H Q and Wang W J 2011 *Solid State Commun.* **151** 499
[31] Jiang L B, Liu Y, Zuo S B and Wang W J 2015 *Chin. Phys. B* **24** 027503
[32] Yan Z, Wu H L, Zheng R S and Xu B S 2015 *Materials Research Innovations* **19** S5-366
[33] Wu Z G, Zhang W B, Hu H R, Zuo S Y, Wang F Y, Yan P X, Wang J, Zhuo R F and Yan D 2014 *Mater. Lett.* **136** 95
[34] Han R L, Jiang S M and Yan Y 2017 *Chin. Phys. B* **26** 027502
[35] Kresse G and J. Furthmüller 1996 *Phys. Rev. B* **54** 11169
[36] Kresse G and Hafner J 1994 *Phys. Rev. B* **49** 14251
[37] Perdew J P, Burke K and Ernzerhof M 1996 *Phys. Rev. Lett* **77** 3865
[38] Blöchl P E 1994 *Phys. Rev. B* **50** 17953
[39] Heyd J, Scuseria G E and Ernzerhof M 2006 *J. Chem. Phys.* **124** 219906
[40] Sahin H, Cahangirov S, Topsakal M, *et al.* 2009 *Phys. Rev. B* **80** 155453
[41] Li S S, Zhang C W, Zhang R W, Li P, Li F, Yuan M, Ren M J, Ji W X and Wang P J 2014 *RSC Adv.* **4** 7500
[42] Zhang C W and Wang P J 2011 *Phys. Lett. A* **375** 3583
[43] Bacaksiz C, Sahin H, Ozaydin H D, *et al.* 2015 *Phys. Rev. B* **91** 085430
[44] Guo H Y, Zhao Y, *et al.* 2012 *J. Phys. Chem. C* **116** 11336
[45] Zhou J, Wang Q, Sun Q and Jena P 2010 *Phys. Rev. B* **81** 085442
[46] Shen L, Wu R Q, Pan H, Peng G W, Yang M, Sha Z D and Feng Y P 2008 *Phys. Rev. B* **78** 073306
[47] Long R and English N J 2009 *Phys. Rev. B* **80** 115212